ISSN 1027-4510, Journal of Surface Investigation: X-ray, Synchrotron and Neutron Techniques, 2023, Vol. 17, No. 1, pp. 208–215. © Pleiades Publishing, Ltd., 2023.
Russian Text © The Author(s), 2023, published in Poverkhnost', 2023, No. 2, pp. 40–48.

Structural and Phase Changes in Concentrated V–Nb–Ta–Ti Solid Solutions Irradiated by Helium Ions

V. V. Uglov[a, *], S. V. Zlotski[a, **], M. M. Belov[a], A. E. Ryskulov[b], K. Jin[c], I. A. Ivanov[b], A. E. Kurakhmedov[b], D. A. Mustafin[b], A. D. Sapar[b], and Y. V. Bikhert[b]

[a] *Belarusian State University, Minsk, 220030 Belarus*
[b] *Institute of Nuclear Physics, Nur-Sultan, 050032 Kazakhstan*
[c] *Beijing Institute of Technology, Beijing, 100811 China*
**e-mail: Uglov@bsu.by*
***e-mail: Zlotski@bsu.by*

Received June 24, 2022; revised July 25, 2022; accepted July 25, 2022

Abstract—The effect of irradiation by low-energy helium ions with a fluence of 2×10^{17} cm^{-2} and an energy of 40 keV on the structure and phase state of V–Nb–Ta–Ti solid solutions is studied to obtain data on the radiation resistance of multicomponent solid solutions promising for use as structural materials of new generation reactors. It is established by scanning electron microscopy and X-ray diffraction analysis that the synthesized binary, ternary, and quaternary V–Nb–Ta–Ti alloys are equiatomic single-phase solid solutions with a uniform element distribution over the surface and compressive microstresses and macrostresses. It is shown that irradiation of the V–Nb–Ta–Ti alloys by helium ions leads to neither the decay of a solid solution nor violation of the uniform equiatomic distribution of elements over the surface. Irradiation by helium ions does not significantly change the level of microstresses and macrostresses in the VNb and VNbTa systems, while in the VNbTaTi alloy the compressive-stress level increases, which can be related to the segregation of elements to grain boundaries and the accumulation of helium-vacancy clusters.

Keywords: high-entropy alloys, multicomponent solid solutions, irradiation, radiation-induced defects, helium ions, residual stress

DOI: 10.1134/S102745102301041X

INTRODUCTION

In recent times, nuclear power is the most efficient source of electricity [1]. As technology advances, so does the need to enhance the efficiency of nuclear reactors. The development of new generation-IV nuclear reactors requires materials that exhibit high mechanical properties at elevated temperatures and a high resistance to radiation exposure during interaction with nuclear-reaction products [2].

Available austenitic steels are inapplicable as new reactor materials because of their strong radiation swelling; the use of ferritic/martensitic steels faces unsolved problems related to creep resistance and embrittlement at irradiation temperatures above 550°C [3–5]. Therefore, the issue of developing new radiation-resistant materials is relevant for the world's research teams.

High-entropy alloys (HEAs) based on a single-phase solid solution and a large number of basic elements in equimolar or almost equimolar ratios are promising for the creation of radiation-resistant materials for nuclear power engineering [6]. HEAs include alloys consisting of five or more elements with a concentration of 5–30 at %. It is commonly believed that maximization of the configurational entropy of HEAs facilitates the formation of a single-phase disordered solid solution instead of the precipitation of complex intermetallic phases; as a result, the alloy has a simple structure with properties better than those of conventional alloys [7–9]. Numerous studies have shown that HEAs have a high elastic limit, fatigue strength, and thermal, corrosion, creep, and radiation resistances [7, 10] attributed to their four main features: high entropy, higher crystal-lattice strain than in conventional metals and alloys, multielement composition, and slow diffusion [10]. A high degree of chemical disorder and lattice distortion in HEAs increase electron and phonon scattering, which leads to a decrease in thermal and electrical conductivity. This results in slower energy dissipation during the collision cascade and an increase in the thermal-spike duration, which enhances the recombination between vacancies and

interstitials [11–13]. In addition, the energies of formation and migration of vacancies and interstitial atoms have a wider distribution, which also enhances the recombination of defects [14–16]. Due to their complex composition, impurity-defect clusters formed during the interaction of point defects move along a chaotic trajectory differing from directed motion in simple metals. This leads to an increase in the number of interstitial clusters in the region enriched with vacancies, which increases the recombination of defects [17, 18].

Most studies on HEAs have been aimed at investigating multicomponent solid solutions with a face-centered cubic (fcc) structure. Therefore, to better understand defect formation and radiation resistance in HEAs, it is important to study HEAs with a body-centered cubic (bcc) structure, in particular, under helium-ion irradiation. High-dose (more than 5×10^{16} cm^{-2}) low-energy irradiation by helium ions increases compressive stresses due to the formation and accumulation of radiation defects, in particular, helium-vacancy clusters. The implantation of gas atoms and formation of radiation defects (interstitial atoms and vacancies) leads to a change in the lattice parameter and the formation of a disordered structure at the surface, which causes transverse stresses in the implanted region. During further irradiation, blisters (bubble-shaped surface defects) form and grow, thereby creating a gap in the metal, which leads to a change in the physical and chemical surface properties and loss of the structural integrity of the material ultimately worsening its characteristics [19, 20].

The aim of this work is to study the structure and phase state of binary, ternary, and quaternary systems of concentrated V–Nb–Ta–Ti solid solutions irradiated by low-energy helium ions.

EXPERIMENTAL

Binary, ternary, and quaternary solid solutions based on the V–Nb–Ta–Ti system were synthesized at the Beijing Institute of Technology from high-purity (>99.9%) metal powders by arc melting with subsequent homogenization and annealing at a temperature of 1150°C for 24 and 72 h with intermediate cold rolling.

The samples were irradiated on a DC-60 heavy ion accelerator at the Astana branch of the Institute of Nuclear Physics (Kazakhstan). Since a great number of neutrons are released during the operation of a nuclear reactor, causing nuclear reactions in the material with the formation of inert gases, He^{2+} ions with an energy of 40 keV and an integral f luence of 2×10^{17} cm^{-2} were chosen for irradiation.

Changes in the structure and phase composition after irradiation were evaluated by X-ray diffraction analysis on a Rigaku Ultima IV diffractometer in a parallel beam geometry using copper radiation (λ = 0.15418 nm). To study only the helium-implanted surface layer, the samples were shot at a fixed small (1°) angle of incidence of X-rays [21]. In this geometry, the X-ray penetration depths for V and the VNb, VNbTa, and VNbTaTi alloys were 284, 146, 72, and 62 nm, respectively [21]. To eliminate the influence of alloy texture, shooting was performed under continuous rotation of the sample at a rate of 30 rpm. The effect of irradiation on the sample structure was studied by changes in the macrostresses (the $\sin^2\psi$ method) and the microstresses (the Halder–Wagner method) [22, 23].

The element distribution in the surface layer and its morphology were examined by scanning electron microscopy (SEM) and energy-dispersive X-ray spectroscopy (EDS) on a ZEISS LEO 1455 VP scanning electron microscope.

The energy loss in the samples under irradiation by helium ions was calculated in the SRIM 2013 program using the Kinchin–Pease model [24]. The threshold displacement energies for elements V, Nb, Ta, and Ti were taken to be 40, 78, 91, and 30 eV, respectively [24]. According to the distribution profiles of implanted He^{2+} ions and the results of radiation-damage simulation (measured by the number of atomic displacements per atom (dpa) in the crystal lattice of a material), the maximum path of helium ions was 325 nm with the maximum damage at a depth of 160–170 nm for vanadium and 120–140 nm for the VNbTaTi alloy (Fig. 1). The highest damaging dose (5.5 dpa) was found for pure vanadium. The VNb and VNbTa samples exhibit a higher peak concentration of implanted He^{2+} ions (23%) as compared with other samples, but the damaging dose is much lower than in V and VNb: 4.4 and 3.8 dpa for VNb and VNbTa, respectively.

RESULTS AND DISCUSSION

The EDS data on the elemental composition of the initial samples are given in Table 1. It can be seen that the samples of the binary, ternary, and quaternary systems are characterized by an equiatomic element ratio (within an error of 5–6%). SEM analysis of the sample surface revealed the uniform structure of the V, VNb, VNbTa, and VNbTaTi samples (Fig. 2). Examination of the element distribution in these samples (Fig. 2) showed that it is uniform over the surface (Fig. 3). Minor deviations from the uniformity of the element distribution are probably due to insufficient homoge-

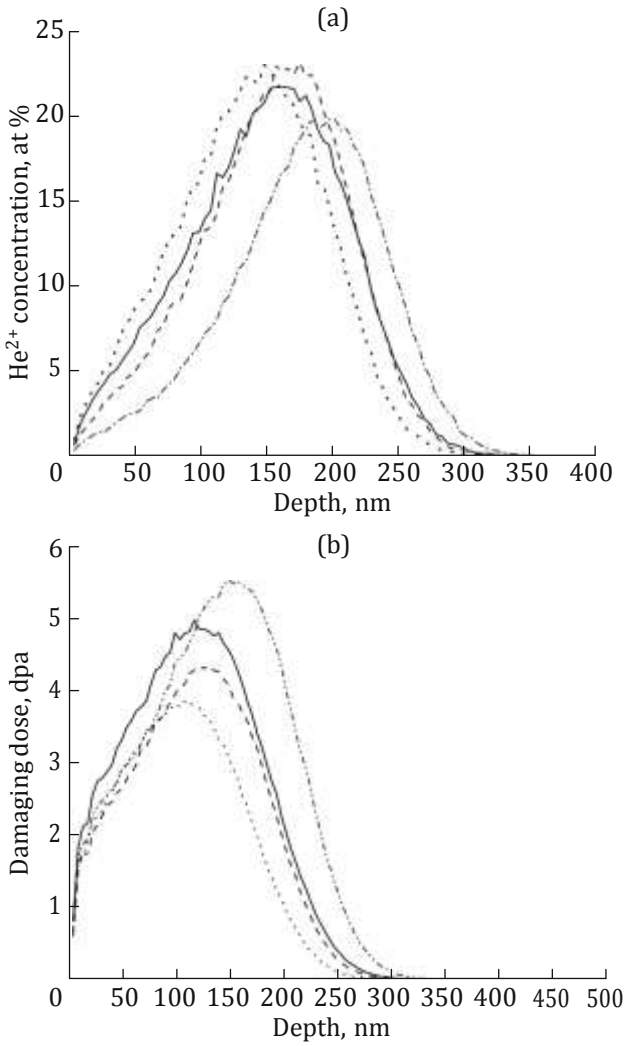

Fig. 1. Depth distribution profiles of (a) He^{2+} ions and (b) a damaging dose in the V (dash-and-dot line), VNb (dashed line), VNbTa (dotted line), and VNbTaTi (solid line) samples irradiated by helium ions with an energy of 40 keV.

nization of the samples and the grain structure of the materials.

According to published data, the equiatomic composition of multicomponent solid solutions can be indicative of the formation of single-phase solid solutions [25]. The X-ray diffraction study confirmed this assumption (Fig. 4). The general view of X-ray diffraction patterns of the unirradiated samples (narrow intense diffraction peaks) points to a high degree of alloy crystallinity and coarse grains; a slight asymmetry of the diffraction lines in more complex systems is related to the possible structural inhomogeneity caused by local inhomogeneity of the alloy elements with different atomic radii of elements, which is typical of high-entropy multicomponent alloys. As can be seen in Fig. 4, all the samples are single-phase solid solutions with a bcc lattice. The lattice parameter of the V, VNb, VNbTa, and VNbTaTi samples increases with the composition complexity and amounts to 0.3027, 0.3177, 0.3227, and 0.3234 nm, respectively. An increase in the lattice parameter is associated with an increase in the atomic radius of elements in the composition.

Table 1. Elemental composition of the initial V–Nb–Ta–Ti system

Sample	Element content, at %			
	V	Nb	Ta	Ti
V	100	–	–	–
VNb	49.5	50.5	–	–
VNbTa	33.9	34.2	31.9	–
VNbTaTi	23.6	26.1	25.9	24.5

Let us consider the behavior of the synthesized samples after irradiation by helium ions with an energy of 40 keV and a fluence of 2×10^{17} cm^{-2}.

The X-ray diffraction patterns of the V, VNb, VNbTa, and VNbTaTi samples irradiated by helium ions show that the phase composition does not change (decomposition of the solid solutions was not detected), but there is a more pronounced asymmetry of the peaks and their shift toward smaller reflection

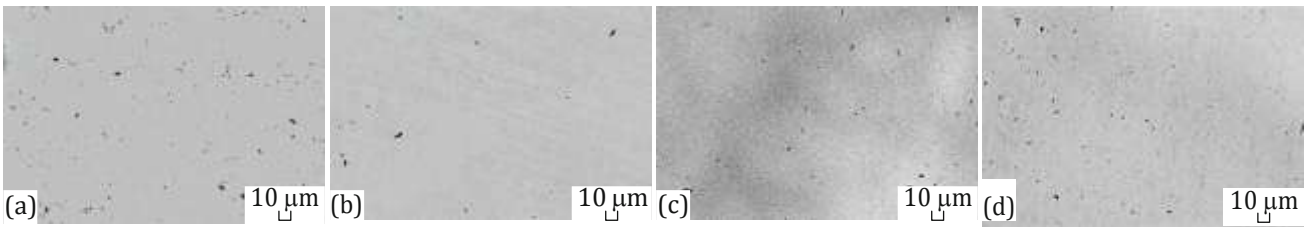

Fig. 2. Surface morphology of the initial (a) V, (b) VNb, (c) VNbTa, and (d) VNbTaTi samples.

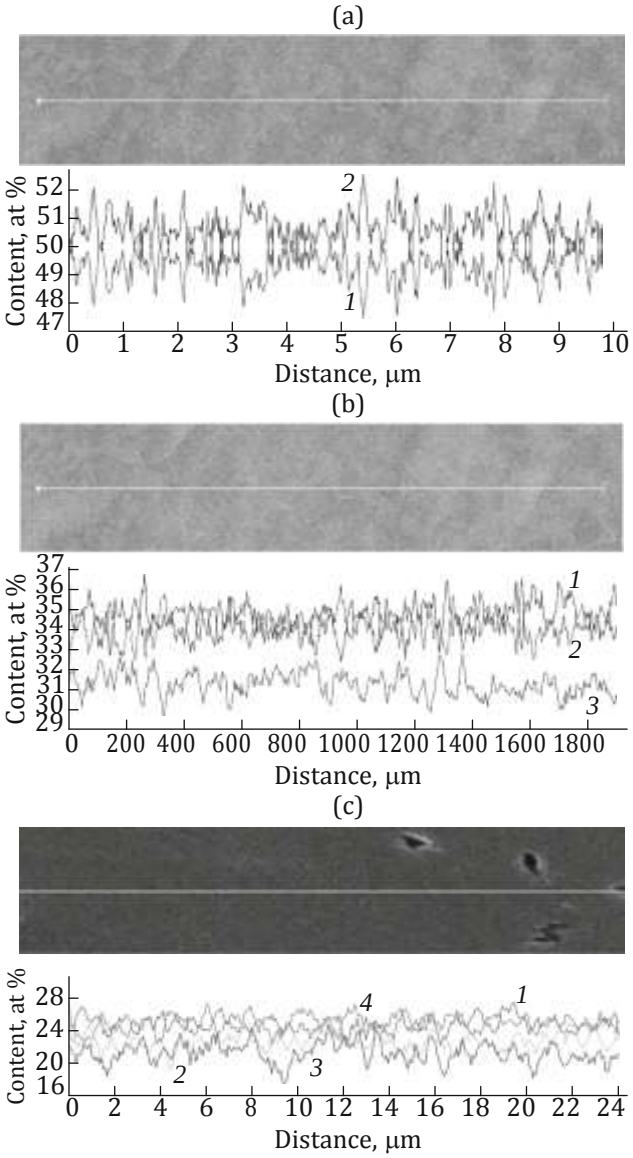

Fig. 3. Distribution profiles of (*1*) V, (*2*) Nb, (*3*) Ta, and (*4*) Ti in the initial (a) VNb, (b) VNbTa, and (c) VNbTaTi samples. The measurements were performed along the white lines marked in the images of the samples.

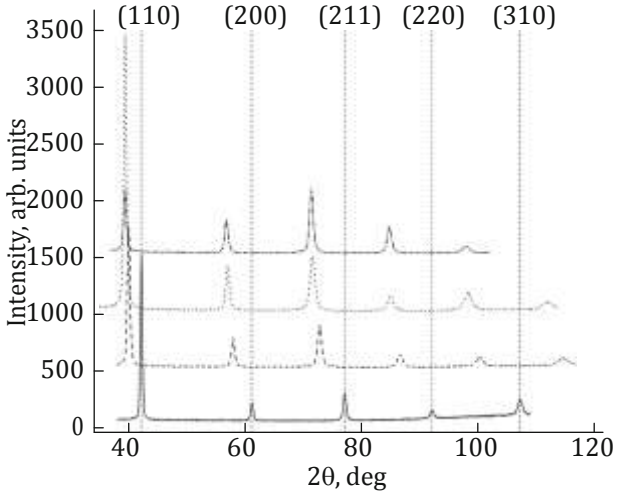

Fig. 4. X-ray diffraction patterns of the initial V (solid line), VNb (dotted line), VNbTa (dash-and-dot line), and VNbTaTi (dashed line) samples.

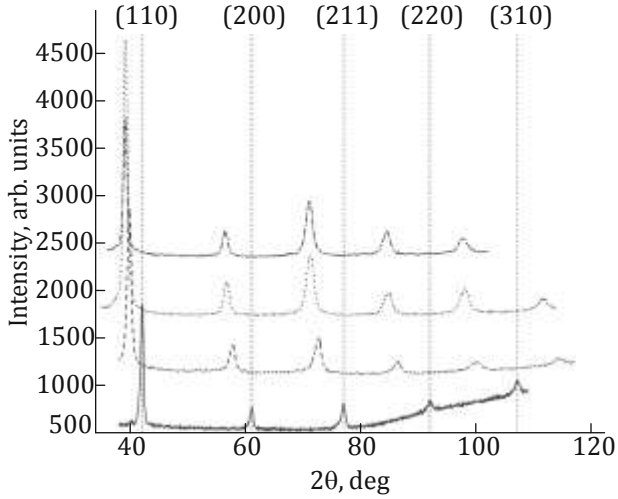

Fig. 5. X-ray diffraction patterns of the V (solid line), VNb (dotted line), VNbTa (dash-and-dot line), and VNbTaTi (dashed line) samples irradiated by He^{2+} ions with an energy of 40 keV.

Table 2. Elemental composition of the V–Nb–Ta–Ti samples irradiated by helium ions with an energy of 40 keV

Sample	Element content, at %			
	V	Nb	Ta	Ti
V	100	–	–	–
VNb	49.4	50.6	–	–
VNbTa	31.7	34.2	34.1	–
VNbTaTi	25.7	25.5	23.7	25.2

angles as compared with the initial X-ray diffraction patterns. This indicates the radiation-induced crystal-lattice strain in the surface region (Fig. 5).

After irradiation, we revealed neither surface changes associated with radiation erosion, nor the surface segregation of elements and violation of uniform distribution (Figs. 6, 7). The equiatomic ratio of the elements was not violated either (Table 2).

To quantitatively estimate the radiation damage, residual macrostresses and microstresses in the initial and irradiated samples were calculated (Figs. 8, 9).

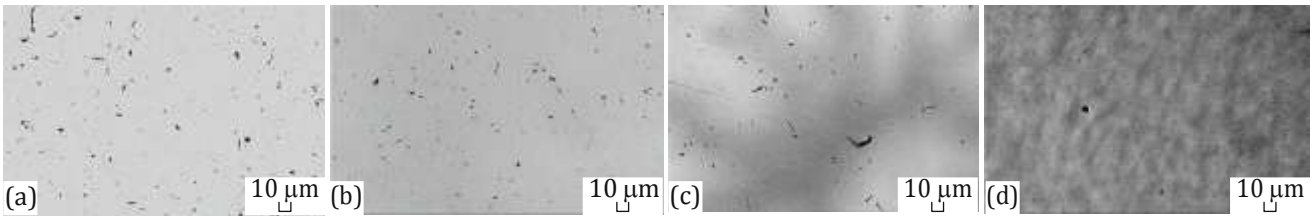

Fig. 6. Surface morphology of (a) the V, (b) VNb, (c) VNbTa, and (d) VNbTaTi samples irradiated by He^{2+} ions with an energy of 40 keV.

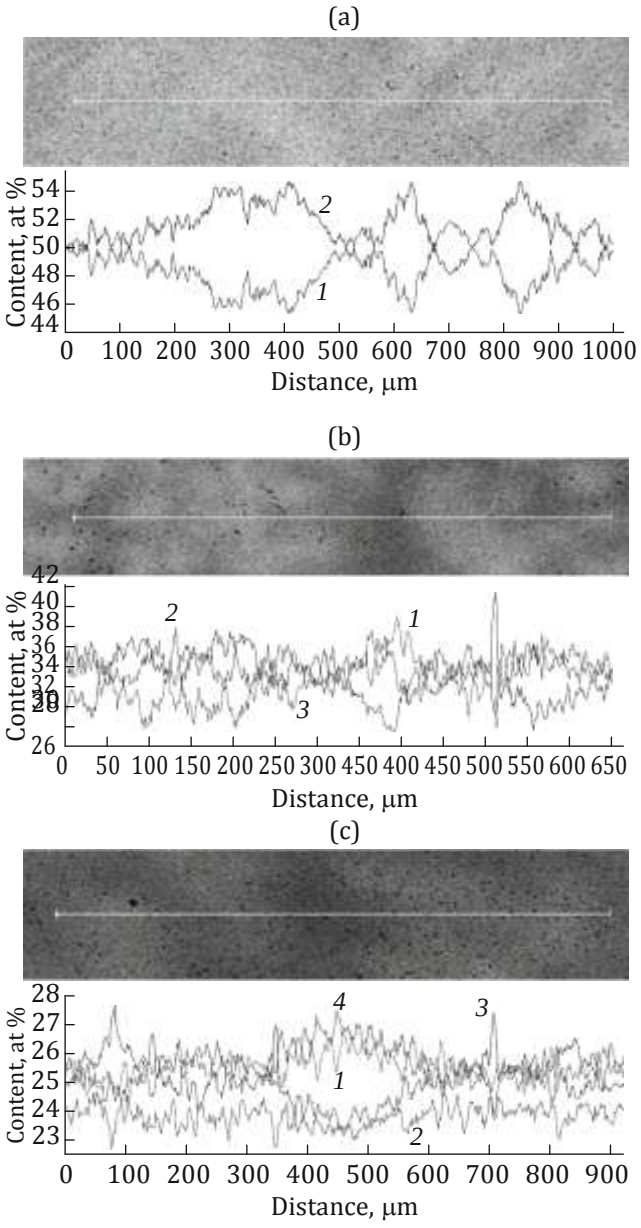

Fig. 7. Distribution profiles of (*1*) V, (*2*) Nb, (*3*) Ta, and (*4*) Ti in (a) the VNb, (b) VNbTa, and (c) VNbTaTi samples irradiated by He^{2+} ions with energy 40 keV.

Figure 8 shows the $\sin^2\psi$ dependences of the interplanar spacings in V and the VNb, VNbTa, and VNbTaTi solid solutions. Macrostresses were determined using the (110) orientation. To find voltage values, the obtained dependences were approximated by a linear function ($v = B - Ax$). Figure 9 presents the stress values obtained. In all the initial samples, compressive stresses dominate. The Nb and Ta additions in the VNb and VNbTa samples increase the compressive-stress level, which is related to the large atomic radii of these elements as compared with V. In the VNbTaTi alloy, due to the presence of Ti, which has a lower melting point and a smaller atomic radius and reduces the modulus of elasticity of the alloy, the compressive-stress level was lower. Irradiation of the vanadium sample by helium ions enhances the compressive macrostress level due to the formation of helium-vacancy clusters, which stretch the material. In addition, microstress relaxation was revealed, which can be attributed to the migration of helium-vacancy clusters toward the grain boundaries [26]. In the VNbTaTi alloy, the microstress and macrostress levels increase as compared with the vanadium sample. Such a significant change in macrostresses can be associated with the use of the grazing geometry of shooting at a small (1°) angle of incidence of X-rays. In this case, due to the small X-ray penetration depth, only the area with the maximum damaging dose and implanted helium-ion concentration is captured, which is the area with the highest stress level. An increase in the microstress level can result from the radiation-induced diffusion of lighter elements toward grain boundaries. This effect was observed previously in multicomponent solid solutions [27–30]. In the VNb and VNbTa alloys, no significant change in the residual stresses was found, which is indicative of the good radiation resistance of these alloys in the VNbTaTi system. The strong crystal-lattice distortion and uniformity of the element distribution are obstacles for the motion of vacancies and helium atoms induced by irradiation, which reduce the helium concentration and diffusion rate and slow the aggregation of helium bubbles [11–

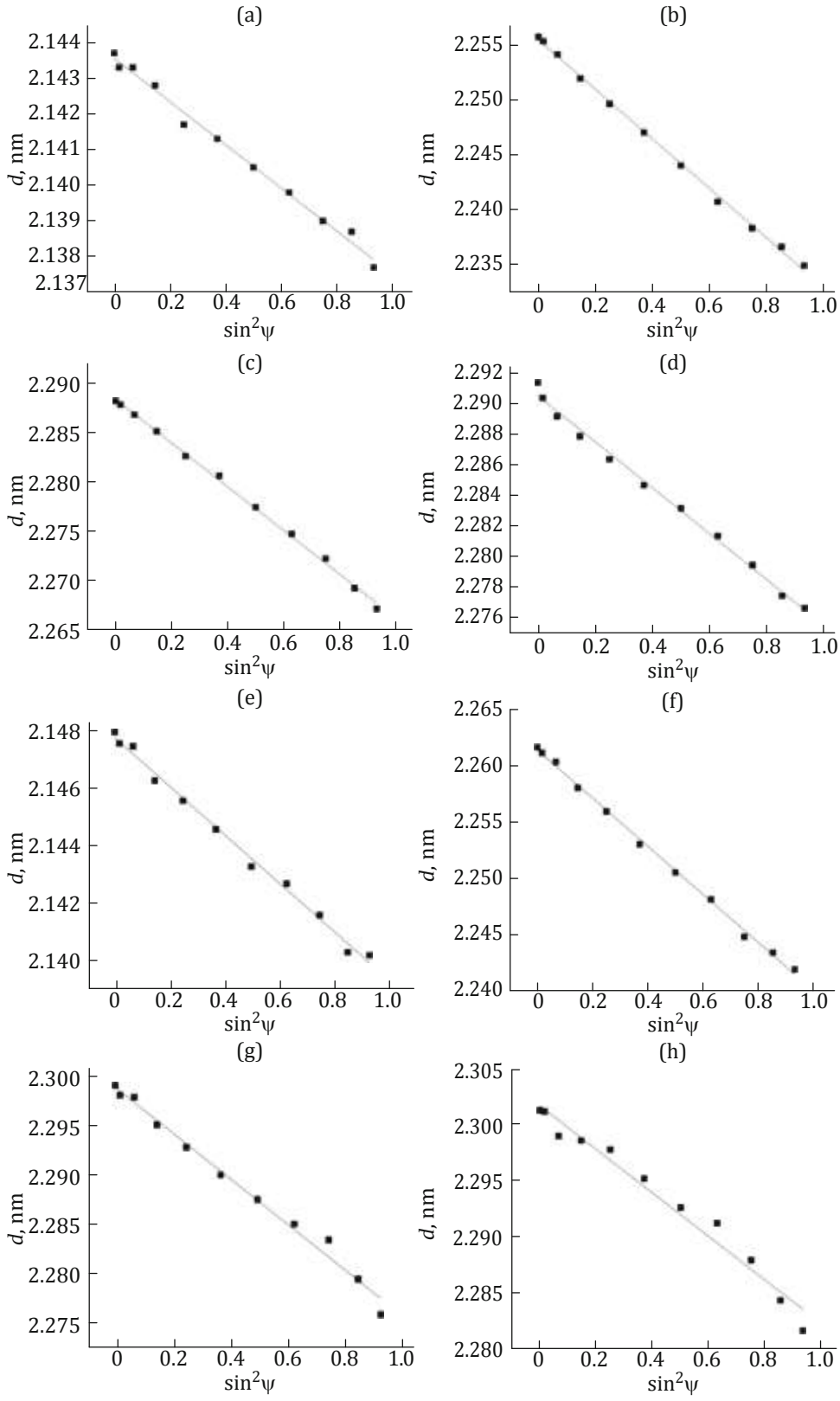

Fig. 8. Macrostress values obtained by the $\sin^2\psi$ method for (a–d) the initial and (e–h) helium-irradiated V–Nb–Ta–Ti samples. The linear approximation coefficients were (a) $A = -0.0061$ and $B = 2.1436$, (b) $A = -0.0225$ and $B = 2.2554$, (c) $A = -0.0222$ and $B = 2.2887$, (d) $A = -0.0150$ and $B = 2.2904$, (e) $A = -0.0084$ and $B = 2.1477$, (f) $A = -0.0213$ and $B = 2.2614$, (g) $A = -0.0230$ and $B = 2.2988$, (h) $A = -0.0195$ and $B = 2.3017$.

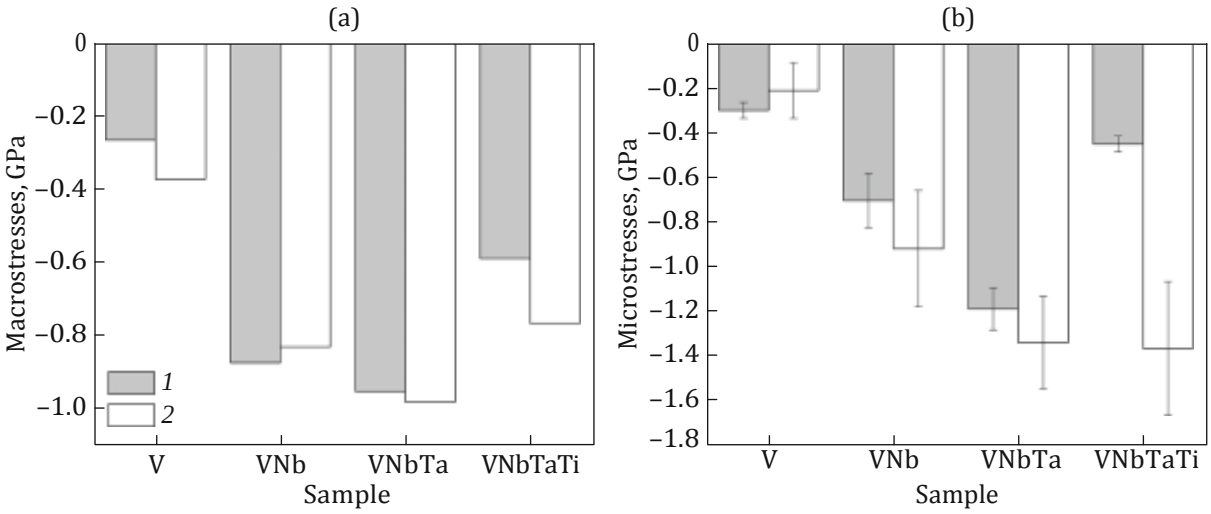

Fig. 9. (a) Macrostress and (b) microstress values in the initial V–Nb–Ta–Ti samples (gray histogram) and the samples irradiated with ions He^{2+} with an energy of 40 keV (white histogram).

13, 31]. Thus, it can be assumed that the properties of the VNbTaTi-based equiatomic multicomponent solid solutions depend not only on the number of elements included in the alloy, but also, to a greater extent, on the characteristics of the constituent elements; this assumption, however, requires further investigations.

CONCLUSIONS

The single-phase equiatomic binary, ternary, and quaternary V–Nb–Ta–Ti solid solutions with a bcc lattice were obtained by arc melting with subsequent homogenization. Before irradiation, compressive stresses were found in the initial materials. The Nb and Ta additions to the alloy were shown to increase the compressive-stress level, while the Ti addition reduced it.

The phase composition and structure of the surface layer of the binary, ternary, and quaternary V–Nb–Ta–Ti-based solid solutions are resistant to irradiation by helium ions with an energy of 40 keV and a fluence of 2×10^{17} cm^{-2}. Irradiation increases significantly the compressive-stress level in the VNbTaTi multicomponent solid solution, which is due to the accumulation of a great number of implanted helium ions and a decrease in microstresses as a result of Ti and V segregation to the grain boundaries. In the VNb and VNbTa alloys, no significant changes in the microstresses and macrostresses were found, which implies the best radiation resistance of these alloys.

CONFLICT OF INTEREST

The authors declare that they have no conflicts of interest.

REFERENCES

1. R. C. Armstrong, C. Wolfram, K. de Jong, et al., Nat. Energy **1**, 15020 (2016). https://doi.org/10.1038/nenergy.2015.20
2. S. J. Zinkle and J. T. Busby, Mater. Today **12**, 12 (2009). https://doi.org/10.1016/S1369-7021(09)70294-9
3. J. Henry and S. A. Maloy, *Structural Materials for Generation IV Nuclear Reactors* (Elsevier, Amsterdam, 2017). https://doi.org/10.1016/B978-0-08-100906-2.00009-4
4. K. Murty and I. Charit, J. Nucl. Mater. **383**, 189 (2008). https://doi.org/10.1016/j.jnucmat.2008.08.044
5. S. J. Zinkle, K. A. Terrani, and L. L. Snead, Curr. Opin. Solid State Mater. Sci. **20**, 401 (2016). https://doi.org/10.1016/j.cossms.2016.10.004
6. K. Jin and H. Bei, Front. Mater. **5**, 1 (2018). https://doi.org/10.3389/fmats.2018.00026
7. J. W. Yeh, Y. L. Chen, S. J. Lin, et al., Mater. Sci. Forum **560**, 1 (2007). https://doi.org/10.4028/www.scientific.net/MSF.560.1
8. M.-H. Tsai and J.-W. Yeh, Mater. Res. Lett. **2**, 107 (2014). https://doi.org/10.1080/21663831.2014.912690
9. Y. Jien-Wei, Ann. Chim. Sci. Mater. **31**, 633 (2006). https://doi.org/10.3166/acsm.31.633-648
10. D. B. Miracle and O. N. Senkov, Acta Mater. **122**, 448 (2017). https://doi.org/10.1016/j.actamat.2016.08.081
11. N. Sellami, A. Debelle, M. W. Ullah, et al., Curr. Opin. Solid State Mater. Sci. **23**, 107 (2019). https://doi.org/10.1016/j.cossms.2019.02.002
12. K. Jin, S. Mu, K. An, et al., Mater. Des. **117**, 185 (2017). https://doi.org/10.1016/j.matdes.2016.12.079

13. E. Zarkadoula, G. Samolyuk, and W. J. Weber, Comput. Mater. Sci. **162**, 156 (2019). https://doi.org/10.1016/j.commatsci.2019.02.039
14. S. Zhao, G. M. Stocks, and Y. Zhang, Phys. Chem. Chem. Phys. **18**, 24043 (2016). https://doi.org/10.1039/C6CP05161H
15. S. Zhao, T. Egami, G. M. Stocks, et al., Phys. Rev. Mater. **2**, 013602 (2018). https://doi.org/10.1103/physrevmaterials.2.013602
16. S. Zhao, Y. Osetsky, and A. V. Barashev, Acta Mater. **173**, 184 (2019). https://doi.org/10.1016/j.actamat.2019.04.060
17. C. Lu, L. Niu, and N. Chen, Nat. Commun. **7**, 13564 (2016). https://doi.org/10.1038/ncomms13564
18. C. Lu, T. Yang, and L. Niu, J. Nucl. Mater. **509**, 237 (2018). https://doi.org/10.1016/j.jnucmat.2018.07.006
19. S. J. Zinkle and G. S. Was, Acta Mater. **61**, 735 (2013). https://doi.org/10.1016/j.actamat.2012.11.004
20. S. Agarwal, P. Trocellier, and Y. Serruys, Nucl. Instrum. Methods Phys. Res., Sect. B **327**, 117 (2014). https://doi.org/10.1016/j.actamat.2016.08.062
21. M. Birkholz, *Thin Film Analysis by X-ray Scattering* (Wiley, New York, 2005).
22. D. Nath, F. Singh, and R. Das, Mater. Chem. Phys. **239**, 122021 (2020). https://doi.org/10.1016/j.matchemphys.2019.122021
23. P. S. Prevey, X-ray diffraction residual stress techniques, in *Materials Characterization*, ASM Handbook, Vol. 10, Ed. by R. E. Whan (ASM Int., 1986), p. 380. https://doi.org/10.31399/asm.hb.v10.a0001761
24. F. Z. James, M. D. Ziegler, and J. P. Biersack, Nucl. Instrum. Methods Phys. Res., Sect. B **268**, 1818 (2010). https://doi.org/10.1016/j.nimb.2010.02.091
25. N. Jia, Y. Li, and H. Huang, Curr. Opin. Solid State Mater. Sci. **550**, 152937 (2021). https://doi.org/10.1016/j.jnucmat.2021.152937
26. R. Kozak, A. Sologubenko, and W. Steurer, Cryst. Mater. **230**, 55 (2015). https://doi.org/10.1515/zkri-2014-1739
27. H. Trinkaus and B. N. Singh, J. Nucl. Mater. **323**, 229 (2003). https://doi.org/10.1016/j.jnucmat.2003.09.001
28. N. Jia, Y. Li, H. Huang, et al., J. Nucl. Mater. **550**, 152937 (2021). https://doi.org/10.1016/j.jnucmat.2021.152937
29. B. Kombaiah, K. Jin, H. Bei, et al., Mater. Des. **160**, 1208 (2018). https://doi.org/10.1016/j.matdes.2018.11.006
30. M. R. He, S. Wang, S. Shi, K. Jin, et al., Acta Mater. **126**, 182 (2017). https://doi.org/10.1016/j.actamat.2016.12.046
31. R. W. Harrison, G. Greaves, H. Le, et al., Curr. Opin. Solid State Mater. Sci. **23**, 100762 (2019). https://doi.org/10.1016/j.cossms.2019.07.001

Translated by E. Bondareva